Journal of the Ceramic Society of Japan 134 [1] 24-30 2026
DOI https://doi.org/10.2109/jcersj2.25119

JCS-Japan

FULL PAPER

Preparation of brookite-type titanium dioxide particle layer on titanium surfaces via hydrothermal treatment and evaluation of *in vitro* apatite-forming ability

Satoshi Hayakawa[1,†], Yushi Nakamoto[2], Seiya Kojima[2], Noriyuki Nagaoka[3], Takuya Kataoka[1] and Tomohiko Yoshioka[1]

[1] Faculty of Interdisciplinary Science and Engineering in Health Systems, Okayama University, 3–1–1 Tsushima-naka, Kita-ku, Okayama 700–8530, Japan
[2] Graduate School of Interdisciplinary Science and Engineering in Health Systems, Okayama University, 3–1–1 Tsushima-naka, Kita-ku, Okayama 700–8530, Japan
[3] Advanced Research Center for Oral and Craniofacial Sciences, Okayama University Dental School, 2–5–1 Shikata-cho, Kita-ku, Okayama 700–8558, Japan

In this study, we prepared a brookite-type titanium dioxide particle layer on the surface of titanium substrates via hydrothermal treatment in aqueous urea solutions containing sodium chloride (NaCl) and examined its *in vitro* apatite-forming ability. Increasing the urea concentration suppressed the formation of anatase-type titanium dioxide on the titanium substrate, forming a particle layer composed of pure brookite-type titanium dioxide. The size and packing density of brookite-type titanium dioxide particles formed on the titanium substrate increased with the NaCl concentration in a 7.0 mol·dm^{-3} urea solution. When titanium substrates hydrothermally treated in aqueous solutions of 7.0 mol·dm^{-3} urea and 2.0 mol·dm^{-3} NaCl were soaked in a simulated body fluid for various periods up to 7 d, the substrate surface was densely covered with hemispherical apatite particles (5.3 μm in diameter) within 3 d, indicating that the brookite-type titanium dioxide particle layer had an excellent apatite-forming ability comparable to that of the anatase-type titanium dioxide particle layer.

Key-words : Brookite-type titanium dioxide, Hydrothermal treatment, Urea, Sodium chloride, Apatite-forming ability

[Received September 5, 2025; Accepted October 21, 2025; Published online November 18, 2025]

1. Introduction

Ti and its alloys are widely used as implant materials in orthopedics and dentistry because of their excellent mechanical properties, corrosion resistance, and biological safety.[1)] However, titanium implant materials have low osteoconductivity and do not easily bond with bone tissue.[2)] Hydroxyapatite (HAp) or carbonate apatite is similar to the inorganic components found in human hard tissues such as teeth and bones, and spontaneously bonds to bone tissue.[3,4)] Therefore, to achieve bonding of titanium-based implants to bone tissue, it is effective to coat their surfaces with HAp particles[5)] or impart an apatite-forming ability on their surfaces.[6)] The combination of chemical treatment with an acidic hydrogen peroxide aqueous solution and heat treatment is one of the techniques used to impart the apatite-forming ability to metallic titanium surfaces. Nanocrystalline titanium dioxide particle layers formed on the titanium surface using this method induce apatite nucleation in simulated body fluid (SBF; Kokubo solution[6)]).[7,8)] Polymorphs of titanium dioxide include anatase (tetragonal), rutile (tetragonal), and brookite (orthorhombic).[9,10)] There are many reports on the *in vitro* apatite-forming ability of titanium dioxide particle layers composed of anatase and rutile phases.[7,8,11,12)] Among the titanium dioxide polymorphs, brookite has not been extensively studied for biomaterials applications. Brookite-type titanium dioxide has been synthesized via hydrothermal treatment of aqueous solutions of water-soluble titanium complexes[13,14)] or aqueous solutions of hydrolyzed products from titanium compounds such as titanium sulfate [$Ti(SO_4)_2$], titanium tetrachloride ($TiCl_4$), titanium trichloride ($TiCl_3$), and tetrabutyl titanate [$Ti(OBu)_4$].[15–18)] It has been synthesized via hydrothermal treatment of metallic titanium powder in an aqueous sodium fluoride solution.[19)] The hydrothermal synthesis of pure brookite-type titanium dioxide from the various aforementioned titanium sources has been achieved using aqueous solutions of urea[14)] or ammonium hydroxide (NH_4OH) in the presence of sodium chloride (NaCl).[17,18)] The objectives of this study were to determine the optimal solution composition for the formation of

† Corresponding author: S. Hayakawa; E-mail: satoshi@okayama-u.ac.jp

brookite-type titanium dioxide particle layers on metallic titanium substrate surfaces via hydrothermal treatment in aqueous urea solutions with various NaCl concentrations and to evaluate the *in vitro* apatite-forming ability of the brookite-type titanium dioxide particle layers.

2. Materials and methods

2.1 Polishing and cleaning of titanium substrates

Pure titanium (cp-Ti) disk (15-mm diameter, 1-mm thickness, GC. Corp. Tokyo, Japan) was polished using a water-resistant SiC polishing paper (#1000) and ultrapure water for 6 min, followed by ultrasonic cleaning three times for 10 min in acetone and once for 10 min in ultrapure water.

2.2 Preparation of aqueous urea solutions containing NaCl

Urea, $(NH_2)_2CO$ powder (Nacalai Tesque Inc. Kyoto, Japan) was dissolved in ultrapure water to prepare 0.5–7.0 $mol \cdot dm^{-3}$ aqueous urea solutions. 7.0 $mol \cdot dm^{-3}$ aqueous urea solutions were prepared by varying the concentration of NaCl (Nacalai Tesque Inc. Kyoto Japan) from 0 to 2.0 $mol \cdot dm^{-3}$.

2.3 Hydrothermal treatment of titanium substrates

Titanium specimens were placed in a 100-cm^3 polytetrafluoroethylene (PTFE) cylindrical container, which was then filled with 20 cm^3 of aqueous urea solutions, and the PTFE container was sealed in a pressure-resistant stainless steel cylindrical container (HU-100, Sanai Kagaku Co. Ltd. Nagoya, Japan). The sealed pressure-resistant container was then stored in a drying oven at 180 °C for 24 h. After hydrothermal treatment, the titanium specimens were sonicated three times in ultrapure water for 10 min.

2.4 Characterization of surface structure

The surface structures of titanium specimens after hydrothermal treatment were analyzed using thin-film X-ray diffraction (TF-XRD). TF-XRD measurements were performed using an X-ray diffractometer (X′Pert-ProMPD, PANalytical, Co. Ltd., Netherlands) with Cu$K\alpha$ radiation ($\lambda = 0.15418$ nm), operating at 45 kV and 40 mA, in the 2θ scanning mode at an incidence angle (θ) of 1.0°. A step size of 0.02° held at 4.00 s/step was used over the measurement range of $2\theta = 20$–40°.

2.5 Evaluation of *in vitro* apatite-forming ability

The titanium specimens were immersed in 30 cm^3 of Kokubo's SBF, which had an ion concentration similar to that of human blood plasma (Na^+ 142.0, K^+ 5.0, Mg^{2+} 1.5, Ca^{2+} 2.5, Cl^- 147.8, HCO_3^- 4.2, HPO_4^{2-} 1.0, SO_4^{2-} 0.5 $mmol \cdot dm^{-3}$).[6] The SBF was prepared by dissolving reagent grade chemicals, such as NaCl, $NaHCO_3$, KCl, $K_2HPO_4 \cdot 3H_2O$, $MgCl_2 \cdot 6H_2O$, $CaCl_2$, Na_2SO_4, and $NH_2C(CH_2OH)_3$ (Nacalai Tesque Inc. Kyoto, Japan) in ultrapure water. The pH was adjusted to 7.40 with tris(hydroxymethyl)aminomethane and 1 $mol \cdot dm^{-3}$ HCl at 36.5 °C. After immersion for 1, 3 and 7 d, the specimens were removed from the fluid, washed with ultrapure water, and then dried in air. The weight of each specimen was measured before and after immersion in the SBF using an electronic balance (XSR205DUV, Mettler-Toledo International Inc. Switzerland). The surface structure of the titanium specimen after immersion in SBF was analyzed using TF-XRD. High magnification scanning electron microscopy (SEM) images of titanium specimens after hydrothermal treatment were obtained using a field emission (FE)-SEM (JSM-IT800, JEOL Ltd., Tokyo, Japan; accelerating voltage of 5 kV, working distance 4 mm). The specimens were coated with high-purity osmium for FE-SEM observation using a Neoc-STB osmium coater (Meiwafosis Co. Ltd., Tokyo, Japan). The surface morphology of the specimens after immersion in SBF was examined using SEM (VE-9800, Keyence Corp., Osaka, Japan; accelerating voltage of 8 kV, spot diameter of 5 mm, working distance 8 mm). Before observation with the SEM, the specimens were coated with platinum to a 30-nm thickness using an ion-beam sputter coater (E-1030, Hitachi Co., Tokyo, Japan). The diameter and surface coverage of the deposited hemispherical apatite particles ($n = 40$) were measured for SEM images using image analysis software (ImageJ, version 1.54g, Wayne Rasband, NIH, Bethesda, MD, USA).

3. Results

3.1 Appearance and surface morphology of titanium specimen after hydrothermal treatment

Figure 1 shows digital photographs of titanium specimens after hydrothermal treatment at 180 °C for 24 h with aqueous solutions of various urea concentrations, indicating the surface color of the specimens for each concentration: (a) yellow at 0.5 $mol \cdot dm^{-3}$, (b) reddish purple at 1.0 $mol \cdot dm^{-3}$, (c) gray at 3.0 $mol \cdot dm^{-3}$, (d) green at 5.0 $mol \cdot dm^{-3}$, and (e) gray at 7.0 $mol \cdot dm^{-3}$.

3.2 Surface structure of titanium specimen after hydrothermal treatment

Figure 2 shows the TF-XRD patterns of titanium specimens after hydrothermal treatment at 180 °C for 24 h with aqueous solutions of various urea concentrations together with the Miller indices (*hkl*) of the XRD peaks based on the ICDD-JCPDS-card. Diffraction peaks attributed to substrate-derived titanium 100 and 002 (PDF#44-1294)

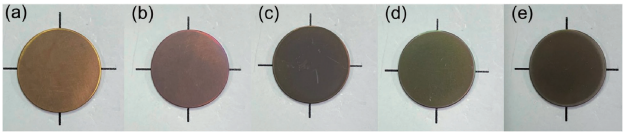

Fig. 1. Digital photographs of titanium specimens after hydrothermal treatment at 180 °C for 24 h in aqueous solutions with various urea concentrations: (a) 0.5 $mol \cdot dm^{-3}$; (b) 1.0 $mol \cdot dm^{-3}$; (c) 3.0 $mol \cdot dm^{-3}$; (d) 5.0 $mol \cdot dm^{-3}$; (e) 7.0 $mol \cdot dm^{-3}$.

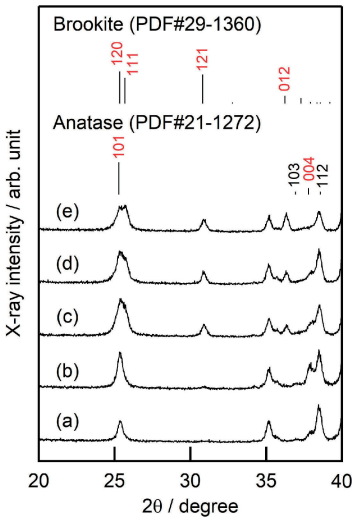

Fig. 2. TF-XRD patterns of titanium specimens after hydrothermal treatment at 180 °C for 24 h in aqueous solutions with various urea concentrations: (a) 0.5 mol·dm^{-3}; (b) 1.0 mol·dm^{-3}; (c) 3.0 mol·dm^{-3}; (d) 5.0 mol·dm^{-3}; (e) 7.0 mol·dm^{-3}.

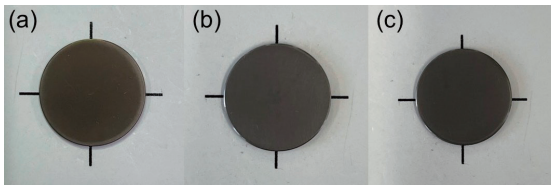

Fig. 3. (A) Digital photographs of titanium specimens after hydrothermal treatment at 180 °C for 24 h in 7.0 mol·dm^{-3} urea aqueous solutions with various NaCl concentrations: (a) 0 mol·dm^{-3}; (b) 1.0 mol·dm^{-3}; (c) 2.0 mol·dm^{-3}.

were observed at $2\theta = 35.1$ and 38.5° for all specimens. Diffraction peaks attributed to anatase 101, 004 (PDF#21-1272) were clearly observed at $2\theta = 25.3$ and 37.8° for titanium specimens treated with aqueous solutions of 0.5 and 1.0 mol·dm^{-3} urea. Diffraction peaks attributed to anatase 101, 004 (PDF#21-1272) and brookite 120, 111, 121, 012 (PDF#29-1360) were observed for titanium specimens treated with aqueous solutions of 3.0 and 5.0 mol·dm^{-3} urea. Diffraction peaks attributed to brookite 120, 111, 121, 012 (PDF#29-1360) were observed at $2\theta = 25.3$, 25.7, 30.9 and 36.3° for titanium specimens treated with aqueous solutions of 7.0 mol·dm^{-3} urea. As the urea concentration increased, the intensity of the diffraction peak corresponding to brookite increased, while the intensity of the diffraction peak corresponding to anatase decreased significantly, indicating that pure brookite-type titanium dioxide was formed in the 7.0 mol·dm^{-3} urea aqueous solution.

Next, we investigated the effect of the addition of NaCl to an aqueous urea solution on the formation of brookite-type titanium dioxide on titanium substrates via hydrothermal treatment. **Figure 3** shows digital photographs of titanium specimens after hydrothermal treatment at 180 °C for 24 h in 7.0 mol·dm^{-3} urea aqueous solutions with various NaCl concentrations, indicating that the surface color of all specimens was gray. These titanium specimens were designated as N0, N1, and N2 according to the NaCl concentration (0, 1.0, 2.0 mol·dm^{-3}, respectively).

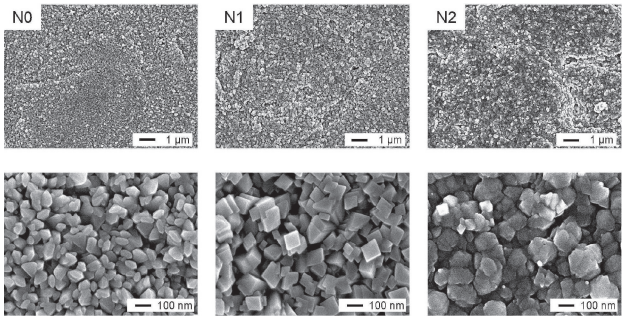

Fig. 4. SEM images of titanium specimens hydrothermally treated in 7.0 mol·dm^{-3} urea aqueous solutions with various NaCl concentrations.

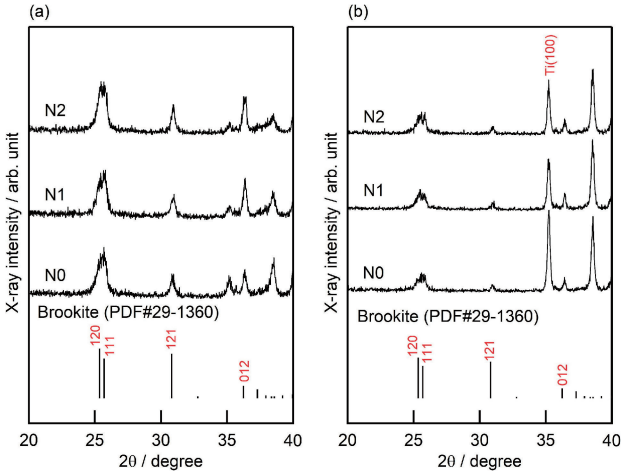

Fig. 5. (a) TF-XRD patterns measured in the 2θ scanning mode and (b) XRD patterns measured in the $2\theta/\theta$ scanning mode for titanium specimens after hydrothermal treatment at 180 °C for 24 h in 7.0 mol·dm^{-3} urea aqueous solutions with various NaCl concentrations.

Figure 4 shows SEM images of titanium specimens hydrothermally treated in 7.0 mol·dm^{-3} urea aqueous solutions with various NaCl concentrations. All specimens exhibited nano-sized particles with characteristic morphology. Specimen N0 showed densely precipitated irregularly shaped particles smaller than 100 nm. Specimen N1 showed rectangular prism shaped particles approximately 100 nm in size. Specimen N2 showed dense precipitation of large secondary particles formed by the aggregation of irregularly shaped nano-particles. These results indicate that the size and packing density of particles increased with the NaCl concentration.

Figure 5 shows the (a) TF-XRD patterns measured in the 2θ scanning mode and (b) XRD patterns measured in the $2\theta/\theta$ scanning mode (b) of titanium specimens after hydrothermal treatment at 180 °C for 24 h in 7.0 mol·dm^{-3} urea aqueous solutions with various NaCl concentrations. Diffraction peaks attributable to titanium and brookite

were observed for all specimens. **Figure 6** shows the intensity ratios of diffraction peak of brookite (*hkl*) to Ti(100) calculated from the profile-fitting and decomposition results of XRD patterns shown in Fig. 5(b). As the NaCl concentration increased, $[I_{\text{brookite(120)}}/I_{\text{Ti(100)}}]$ and $[I_{\text{brookite(012)}}/I_{\text{Ti(100)}}]$ increased.

3.3 Surface structure of titanium specimens after immersion in SBF

Figure 7 shows the TF-XRD patterns of titanium specimens hydrothermally treated in 7.0 mol·dm^{-3} urea aqueous solutions with various NaCl concentrations after immersion in SBF for 1–7 d. For titanium specimen N0, diffraction peaks attributable to apatite 002, and 211 (PDF#09-0432) were observed at $2\theta = 26°$ and 32° after soaking in SBF for 7 d. For specimens N1 and N2, diffraction peaks corresponding to apatite were observed after soaking in SBF for 3 d. The intensity of the diffraction peaks attributable to apatite increased with the immersion time.

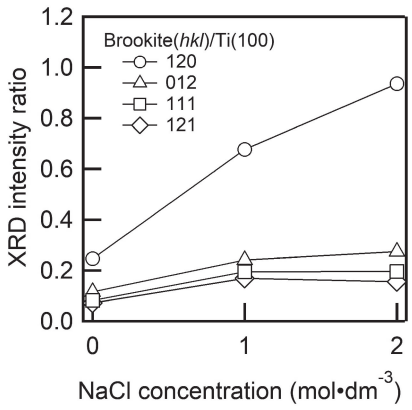

Fig. 6. Diffraction peak intensity ratios of brookite (*hkl*) to Ti(100) as a function of NaCl concentration for titanium specimens hydrothermally treated at 180 °C for 24 h in 7.0 mol·dm^{-3} urea aqueous solutions.

3.4 Weight gain of titanium specimens after immersion in SBF

The weight gain caused by SBF immersion reflects the deposition of apatite particles. **Figure 8** shows the weight gain results of SBF immersion experiments for titanium specimens hydrothermally treated in 7.0 mol·dm^{-3} urea aqueous solutions with various NaCl concentrations. The weight of all specimens increased with immersion time. This result is consistent with the increased intensity of the diffraction peaks assigned to apatite in the XRD patterns shown in Fig. 7.

3.5 Surface morphology of titanium specimens after immersion in SBF

Figure 9 shows SEM images of titanium specimens hydrothermally treated in 7.0 mol·dm^{-3} urea aqueous solutions with various NaCl concentrations after immersion in SBF for 1–7 d. The diameter and surface coverage of the deposited hemispherical particles were summarized in **Table 1**. For specimens N0 and N1, the surface morphology after 1 d of SBF immersion was identical to that of the substrate surface before SBF immersion. For specimen N0,

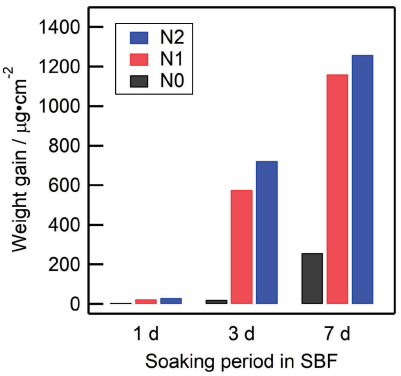

Fig. 8. Weight gain due to SBF immersion of titanium specimens hydrothermally treated in 7.0 mol·dm^{-3} urea aqueous solutions with various NaCl concentrations.

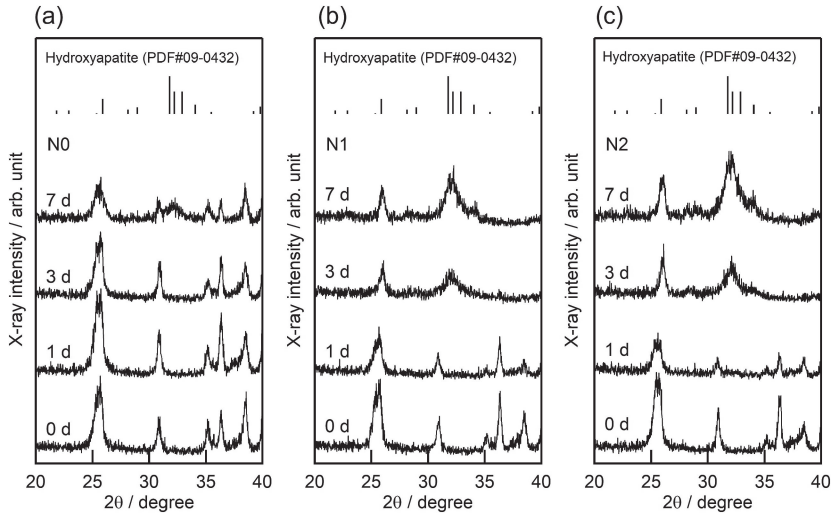

Fig. 7. TF-XRD patterns of titanium specimens hydrothermally treated at 180 °C for 24 h in 7.0 mol·dm^{-3} urea aqueous solutions before and after immersion in SBF for 1–7 d.: (a) N0; (b) N1; (c) N2.

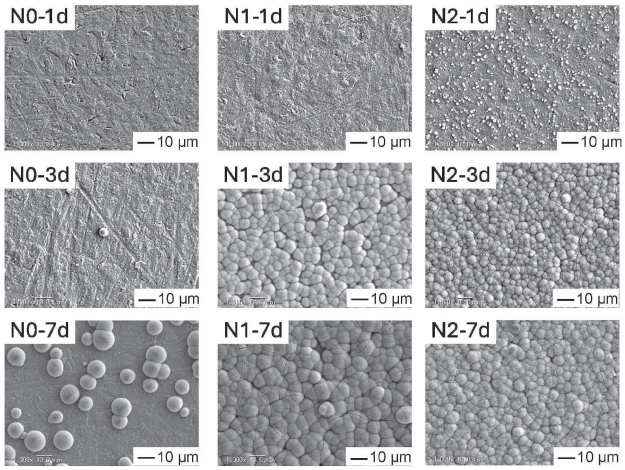

Fig. 9. SEM images of titanium specimens hydrothermally treated in 7.0 mol·dm^{-3} urea aqueous solutions with various NaCl concentrations after immersion in SBF for 1–7 d.

Table 1. Particle diameter and surface coverage

Sample code	Particle diameter (μm)	Surface coverage (%)
N0-7d	9.4 ± 2.7	26.9
N1-3d	7.2 ± 0.7	90.4
N1-7d	7.8 ± 1.4	92.8
N2-3d	5.3 ± 0.8	93.6
N2-7d	5.7 ± 0.8	95.1

hemispherical particles and the substrate surface were observed after soaking in SBF for 7 d. After soaking specimen N1 in SBF for 3d, approximately 90.4 % of the N1 specimen surface was covered with hemispherical particles approximately 7.2-μm in diameter. After soaking specimen N2 in SBF for 1 d, hemispherical particles with diameter of approximately 2-μm or less were observed. After 3d of immersion, approximately 93.6 % of the N2 specimen surface was covered with hemispherical particles approximately 5.3-μm in diameter. These hemispherical particles were smaller and more densely formed than those in specimens N0 and N1.

4. Discussion

4.1 Effect of urea and NaCl on the formation of titanium dioxide

As urea concentration increased, the intensity of the diffraction peak corresponding to anatase decreased significantly, whereas that of the diffraction peak corresponding to brookite did not decrease. (Fig. 2) This indicated that high concentrations of urea inhibited the formation of anatase but not brookite. Under hydrothermal conditions, the decomposition of urea produced NH_4OH and H_2CO_3, followed by the dissociation of these reaction products to form OH^- and CO_3^{2-} ions. These byproducts give the aqueous solution weak basicity (pH 9–10), depending on the initial concentration of urea. Weakly basic aqueous solutions are advantageous for the formation of brookite-type titanium dioxide on titanium substrates. With increasing NaCl concentration, the diffraction peak intensity ratios of brookite TiO_2(*hkl*) to Ti(100), i.e., [$I_{\text{brookite}(120)}/I_{\text{Ti}(100)}$] and [$I_{\text{brookite}(012)}/I_{\text{Ti}(100)}$], increased. (Fig. 6) This suggests that the addition of NaCl to the aqueous urea solutions promoted the formation of brookite-type titanium dioxide particles while inhibiting the formation of anatase-type titanium dioxide particles due to the high concentration of urea.

4.2 *In vitro* apatite-forming ability of brookite-type titanium dioxide particle layer

From the TF-XRD analysis (Fig. 7), weight gain caused by SBF immersion (Fig. 8), and SEM observation (Fig. 9) of the titanium specimens after immersion in SBF, more apatite particles were deposited on the titanium specimens hydrothermally treated with aqueous urea solutions of higher NaCl concentrations. This is attributed to the increase in the size and packing density of brookite-type titanium dioxide particles formed on the surface of the titanium specimens owing to the increase in NaCl concentration. It has been suggested that the lattice matching between the thermodynamically stable surface of crystalline TiO_2 (anatase and rutile) and apatite is important for inducing apatite nucleation in SBF[8,20] and that the hydrated TiO_2 particles exhibits Ti-OH groups involved in the nucleation of apatite.[21,22] Gong and Selloni reported that the most stable brookite TiO_2(210) surface of all brookite surfaces appears as a distorted anatase TiO_2(101) surface and that the surface energy of brookite TiO_2(210) exceeds that of the most stable anatase TiO_2(101).[23,24] Holmström et al. reported a model for the surface hydration structure of brookite TiO_2(210), which has a higher degree of hydroxylation than anatase TiO_2(101).[25] Therefore, the strong hydroxylation of brookite surfaces is expected to have an *in vitro* apatite-forming ability comparable to that of anatase surfaces.

In the apatite formation process proposed by Uetsuki et al.[26] according to results confirming the existence of virtual nucleation sites, the total number of hemispherical particles corresponds to the number of active sites involved in the primary nucleation process of apatite on the surface. Hayakawa et al. proposed a two-dimensional close-packed model for a hemispherical apatite particle layer and derived the following equation for the density of active sites for apatite nucleation and growth:[27]

$$\text{Active-site density (site number/m}^2) = (\sqrt{3}r^2)^{-1} \quad (1)$$

where r represents the diameter of hemispherical apatite particles estimated via SEM image analysis.

SEM images of the surfaces of the chemically prepared titanium dioxide layers after immersion in SBF were extracted from previously published reports.[28–33] Since the maximum surface coverage of hemispherical particles on a flat substrate calculated using the close-packed model is 90.6 %, it is essential to extract SEM images with the surface coverage of 90 % or higher from the reports. As shown in **Fig. 10**, the particle diameter increases mono-

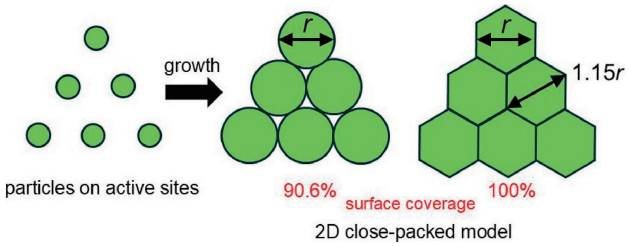

Fig. 10. 2D close-packed model.

tonically with the immersion time in SBF until the close-packed structure is formed. After the formation of close-packed structure, the narrow gaps between hemispherical particles inhibit further lateral particle growth along the specimen surface, causing the rate of increase in particle diameter to decrease to 15 % or less.

When the surface coverage exceeds 93 %, new particles formed on the surface of existing particles or adjacent particles fused to form larger particles (see Fig. 9, N1-7d, N2-7d), making the close-packed model inapplicable. Therefore, these large particles observed on the hemispherical particle layer must be excluded from the calculation of particle diameter. In addition, specimens with low apatite-forming ability were excluded from analysis because they failed to form the close-packed structure, resulting in large particles sparsely distributed on the specimen surface. Considering the above conditions, the diameters of the hemispherical apatite particles were estimated via SEM image analysis to calculate the active-site density. The calculated active-site density is plotted as a function of the diameter of the hemispherical apatite particles in **Fig. 11**. When a larger number of apatite nuclei formed heterogeneously on the surface of the titanium dioxide layer, the surface tended to be coated with smaller-diameter hemispherical apatite particles. However, titanium dioxide coatings fabricated on non-titanium substrate surfaces have a lower active-site density, i.e., rutile-type titanium dioxide coatings prepared on PTFE ($1.17 \times 10^{10}\,m^{-2}$)[28] and anatase-type titanium dioxide coating prepared on titanium alloy (Ti6Al4V) substrate via liquid phase deposition technique ($4.21 \times 10^{9}\,m^{-2}$).[27] In contrast, the calculated active-site density of anatase-type titanium dioxide particle layer prepared via the hydrothermal oxidation was $2.95 \times 10^{11}\,m^{-2}$ (anatase + GRAPE®),[29] which is the maximum value in Fig. 11. This result indicates that the ability to induce apatite nucleation can be amplified by parallel alignment of hydrothermally oxidized cp-Ti substrates separated by sub-millimeter gaps (GRAPE®).[29] Furthermore, it was suggested that diameter of hemispherical particles of the close-packed structure depends not only on the immersion time in SBF but also on the active-site density.

The calculated active-site density of the surface of N2(3d) was $2.13 \times 10^{10}\,m^{-2}$, which exceeded that of N1(3d) ($1.11 \times 10^{10}\,m^{-2}$). The brookite-type titanium dioxide particle layer prepared via hydrothermal treatment (N2) exhibited a moderate amount of active sites between the titania hydrogel derived from the sodium titanate layer

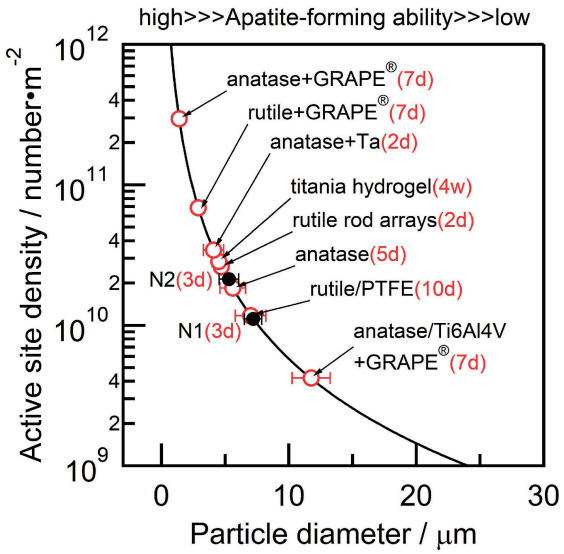

Fig. 11. Relationship between the particle diameter and the density of active sites for apatite nucleation and growth (active-site density). For comparison, the active-site density calculated using the particle diameter obtained from the image analysis of previously reported SEM images is also shown: anatase/Ti6Al4V + GRAPE®,[27] rutile + GRAPE®,[27] rutile/PTFE,[28] anatase + GRAPE®,[29] titania hydrogel,[30,31] anatase,[32] anatase + Ta[20] and rutile rod arrays.[33] The numbers in parentheses of the sample code represent the soaking period in the SBF.

prepared via chemical treatment with an NaOH aqueous solution and subsequent heat treatment at 600 °C ($2.85 \times 10^{10}\,m^{-2}$)[30,31] and the anatase-type titanium dioxide particle layer prepared via chemical treatment with an H_2O_2/HCl aqueous solution and subsequent heat treatment at 400 °C ($1.84 \times 10^{10}\,m^{-2}$) (anatase).[32]

5. Conclusions

Commercially pure Ti substrates were hydrothermally treated in aqueous urea solutions with various NaCl concentrations. TF-XRD analyses of the titanium specimens confirmed that the formation of anatase-type titanium dioxide was suppressed by increasing the urea concentration, whereas the formation of brookite was not. XRD and SEM analyses revealed that the size and packing density of brookite-type titanium dioxide particles formed on the titanium substrate increased with the NaCl concentration in a $7.0\,mol \cdot dm^{-3}$ urea solution. *In vitro* evaluation of the apatite-forming ability revealed that the brookite-type titanium dioxide particle layer was densely covered with hemispherical apatite particles within 3 d, indicating that it had an excellent apatite-forming ability comparable to that of the anatase-type titanium dioxide particle layer.

Acknowledgement This study was supported by JSPS KAKENHI (Grant JP24K08202).

References

1) M. Geetha, A. K. Singh, R. Asokamani and A. K. Gogia, *Prog. Mater. Sci.* 54, 397 (2009).
2) T. Albrektsson, P. I. Branemark, H. A. Hansson, B.

Kasemo, K. Larsson, I. Lundström, D. H. McQueen and R. Skalak, *Ann. Biomed. Eng.* 11, 1 (1983).
3) M. Neo, S. Kotani, Y. Fujita, T. Nakamura, T. Yamamuro, Y. Bando, C. Ohtsuki and T. Kokubo, *J. Biomed. Mater. Res.* 26, 255 (1992).
4) M. Neo, T. Nakamura, C. Ohtsuki, T. Kokubo and T. Yamamuro, *J. Biomed. Mater. Res.* 27, 999 (1993).
5) A. Shikha, S. K. Pandey, E. Arunan and C. Srivastava, *J. Mater. Chem. B* 9, 228 (2021).
6) T. Kokubo and H. Takadama, *Biomaterials* 27, 2907 (2006).
7) X. X. Wang, S. Hayakawa, K. Tsuru and A. Osaka, *J. Biomed. Mater. Res.* 54, 172 (2000).
8) J. M. Wu, S. Hayakawa, K. Tsuru and A. Osaka, *J. Am. Ceram. Soc.* 87, 1635 (2004).
9) X. Bokhimi, A. Morales, M. Aguilar, J. A. Toledo-Antonio and F. Pedraza, *Int. J. Hydrogen Energ.* 26, 1279 (2001).
10) U. Diebold, *Surf. Sci. Rep.* 48, 53 (2003).
11) T. Kokubo, T. Matsushita and H. Takadama, *J. Eur. Ceram. Soc.* 27, 1553 (2007).
12) X. Cui, H.-M. Kim, M. Kawashita, L. Wang, T. Xiong, T. Kokubo and T. Nakamura, *Dent. Mater.* 25, 80 (2009).
13) K. Tomita, V. Petrykin, M. Kobayashi, M. Shiro, M. Yoshimura and M. Kakihana, *Angew. Chem. Int. Edit.* 45, 2378 (2006).
14) T. A. Kandiel, A. Feldhoff, L. Robben, R. Dilert and D. W. Bahnemann, *Chem. Mater.* 22, 2050 (2010).
15) Y. Zheng, E. Shi, S. Cui, W. Li and X. Hu, *J. Am. Ceram. Soc.* 83, 2634 (2000).
16) J. G. Li, C. Tang, D. Li, H. Haneda and T. Ishigaki, *J. Am. Ceram. Soc.* 87, 1358 (2004).
17) X. Shen, B. Tian and J. Zhang, *Catal. Today* 201, 151 (2013).
18) B. Zhao, F. Chen, Q. Huang and J. Zhang, *Chem. Commun.* 34, 5115 (2009).
19) T. Oota, I. Yamai and H. Saito, *Yogyo-Kyokai-Shi* 87, 375 (1979).
20) X. X. Wang, S. Hayakawa, K. Tsuru and A. Osaka, *J. Biomed. Mater. Res.* 52, 171 (2000).
21) P. Li, C. Ohtsuki, T. Kokubo, K. Nakanishi, N. Soga and K. De Groot, *J. Biomed. Mater. Res.* 28, 7 (1994).
22) C. Ohtsuki, H. Iida, S. Hayakawa and A. Osaka, *J. Biomed. Mater. Res.* 35, 39 (1997).
23) X. Q. Gong and A. Selloni, *Phys. Rev. B* 76, 235307 (2007).
24) W.-K. Li, X.-Q. Gong, G. Lu and A. Selloni, *J. Phys. Chem. C* 112, 6594 (2008).
25) E. Holmström, S. Ghan, H. Asakawa, Y. Fujita, T. Fukushina, S. Kamimura, T. Ohno and A. S. Foster, *J. Phys. Chem. C* 121, 20790 (2017).
26) K. Uetsuki, S. Nakai, Y. Shirosaki, S. Hayakawa and A. Osaka, *J. Biomed. Mater. Res. A* 101A, 712 (2013).
27) S. Hayakawa, Y. Masuda, K. Okamoto, Y. Shirosaki, K. Kato and A. Osaka, *J. Mater. Sci.-Mater. M.* 25, 375 (2014).
28) J.-M. Wu, J.-F. Liu, S. Hayakawa, K. Tsuru and A. Osaka, *J. Mater. Sci.-Mater. M.* 18, 1529 (2007).
29) S. Hayakawa, K. Okamoto and T. Yoshioka, *J. Asian Ceram. Soc.* 7, 90 (2019).
30) T. Kokubo, F. Miyaji, H.-M. Kim and T. Nakamura, *J. Am. Ceram. Soc.* 79, 1127 (1996).
31) H.-M. Kim, F. Miyaji, T. Kokubo and T. Nakamura, *J. Biomed. Mater. Res.* 32, 409 (1996).
32) X.-X. Wang, S. Hayakawa, K. Tsuru and A. Osaka, *Biomaterials* 23, 1353 (2002).
33) X. Liu, T. Yoshioka and S. Hayakawa, *J. Asian Ceram. Soc.* 8, 29 (2019).